

Discrete Cosine Transform Network for Guided Depth Map Super-Resolution

Zixiang Zhao, Jiangshe Zhang*, Shuang Xu, Chunxia Zhang, Junmin Liu
Xi'an Jiaotong University
Xi'an, Shaanxi, P.R. China

{zixiangzhao, shuangxu}@stu.xjtu.edu.cn
{jszhang, cxzhang, junminliu}@mail.xjtu.edu.cn

Abstract

Guided depth super-resolution (GDSR) is a hot topic in multi-modal image processing. The goal is to use high-resolution (HR) RGB images to provide extra information on edges and object contours, so that low-resolution depth maps can be upsampled to HR ones. To solve the issues of RGB texture over-transferred, cross-modal feature extraction difficulty and unclear working mechanism of modules in existing methods, we propose an advanced Discrete Cosine Transform Network (DCTNet), which is composed of four components. Firstly, the paired RGB/depth images are input into the semi-coupled feature extraction module. The shared convolution kernels extract the cross-modal common features, and the private kernels extract their unique features, respectively. Then the RGB features are input into the edge attention mechanism to highlight the edges useful for upsampling. Subsequently, in the Discrete Cosine Transform (DCT) module, where DCT is employed to solve the optimization problem designed for image domain GDSR. The solution is then extended to implement the multi-channel RGB/depth features upsampling, which increases the rationality of DCTNet, and is more flexible and effective than conventional methods. The final depth prediction is output by the reconstruction module. Numerous qualitative and quantitative experiments demonstrate the effectiveness of our method, which can generate accurate and HR depth maps, surpassing state-of-the-art methods. Meanwhile, the rationality of modules is also proved by ablation experiments.

1. Introduction

Benefiting from the popularity of consumer-level depth prediction sensors, *e.g.*, Time-of-Flight (ToF) and Kinect cameras, the wide application of depth maps has promoted advancements in areas such as autonomous driving, pose estimation, virtual reality, robot navigation and scene under-

*Corresponding author.

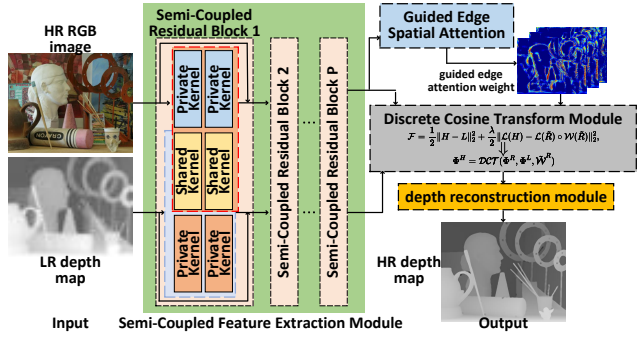


Figure 1. Workflow of our DCTNet.

standing. Unfortunately, due to the technical limitations and the diversity of imaging environments, depth images often have the disadvantages of low-resolution (LR) and noise. However, in the same scene, with the acquisition of depth images, high-resolution (HR) and clear RGB images (or say, intensity images) are relatively easy to obtain. Accordingly, RGB images guided depth map super-resolution, short for the GDSR, has become a hot issue in the area of multi-modal image processing and multi-modal super-resolution (SR). We hope to use the basic assumption that there are statistical co-occurrences between the texture edges of RGB images and the discontinuities of depth maps [26]. In this way, the information contained in RGB images can be utilized to improve the accuracy of depth prediction and obtain an advanced depth map with higher quality than the violent upsampling schedule.

For the color image SR task, machine learning models have achieved a dominant effect by learning a mapping from LR to HR images [5, 18]. However, the SR of color images mainly focuses on feature extraction and reconstruction of details and textures. Differently, DSR tasks mainly need to infer textureless and piecewise affine regions that have sharp depth discontinuities [26]. In addition, depth maps tend to be noisy and have a lower tolerance for artifacts in real-world application [31]. Thus, the methods for RGB

images SR cannot be directly grafted to the depth map SR effectively and the completion of the GDSR task requires attention to its unique characteristics. Roughly speaking, for GDSR task, conventional methods¹ can be divided into three categories, *i.e.*, filter-, optimization- and learning-based methods. Filter-based (or local) methods [19, 23, 22, 21], are affected by joint bilateral upsampling [14, 1] and its variants [14]. The purpose is to implement edge awareness and to preserve sharpened depth edges under the guidance of the intensity image. These methods usually have lower computational complexity and higher computational efficiency, but for texture-rich RGB images, irrelevant edges may be transferred to depth images, which is difficult to form an effective guide. In addition, the explicitly defined filter kernel can only model a specific visual task, and it is difficult to improve the algorithm framework and process coherently. For optimization-based (or global) methods [4, 24, 33, 6, 17], by manually designing energy functional based on diverse data prior, the data fidelity term makes the solution accords with the degradation process and regularization term constraint the solution space [35]. The reconstruct HR depth map is obtained as the optimal solution. A critical step to this type of method is whether it can design an optimization function that meets the task characteristics. But in fact, natural priors are often difficult to be explicitly represented and learned. The third category are the learning-based methods [32, 8, 31], which mainly employ data-driven pipelines to learn the dependency representation between multi-modal input images. The representative methods are based on sparse dictionary learning [13, 28, 15], which learn dictionaries in a group learning manner with paired depth/RGB patches and set constraints on the sparse representations of different modalities [35, 3]. Learning-based methods can effectively adapt to the characteristics of various data modalities, but the computational cost of learning a dictionary is relatively expensive.

In the era of deep learning (DL), as the most popular tool for learning-based methods, various DL architectures are used to learn the mapping from LR to HR images [16, 12, 9, 3, 2]. In addition, DL architectures often cooperate with the other two categories of methods to complete depth upsampling tasks. For example, the learnable filter models [30] (the combination of DL and filter) and the algorithm unrolling models [25] (the combination of DL technology and optimization method) have shown good results and development potential. However, some challenges in the conventional methods, *e.g.*, the edge mismatch or over-transferred between the RGB/depth image, the difficulty for effective learning of natural priors and the poor flexibility of models, along with the shortcomings of deep learning to explain the internal working mechanism, are still expect to be completely resolved.

In response to the above-mentioned challenges, and inspired by coupled dictionary learning in sparse coding and the physics-based modeling ideas, we propose a Discrete Cosine Transform Network (DCTNet) for the GDSR task. Its workflow can be seen in Fig. 1. Our DCTNet consists of four components, namely semi-coupled feature extraction that containing four semi-coupled residual blocks, a guided edge spatial attention (GESA) module, a discrete cosine transform (DCT) module and a depth reconstruction module. First, the LR depth map and the HR RGB image are paired into the encoder, and semi-coupled residual blocks are used to extract shared/private features from the source images. The RGB feature is then employed by the GESA module to obtain the edge attention weights useful for SR. Subsequently, multi-channel RGB/depth features and the edge attention weights are input into the DCT module to acquire HR depth features, and the final predicted HR depth map is reconstructed by the decoder. Our contribution can be summarized as follows:

Firstly, we believe that depth/RGB image pair in the same scene will have a correlation between the intensity edge and the depth discontinuities, while each has its own private features in terms of texture details or segmented smoothness. Therefore, we establish an effective feature extraction encoder which integrates four semi-coupled residual blocks. In each convolutional layer of this module, half of the convolution kernels are responsible for extracting shared features in depth/RGB images, whose parameters are shared. On the contrary, the other half of the convolution kernels are employed to extract the individual features in the depth/RGB image, *i.e.*, the unique features that are different from each other. Parameters in the private encoders are not shared. With residual connection, the feature extraction encoder can effectively extract the features required by GDSR from input image pairs.

Secondly, we propose an advanced DCT module to alleviate the unexplainable and unclear internal working mechanisms in the empirical-designed DL architecture. The module utilizes DCT to solve a well-designed optimization model for GDSR, and implants it in the DNN structure as a module to achieve the acquisition of HR depth map features guided by RGB features in the multi-channel feature domain. Therefore, our DCTNet does not need to focus on LR/HR mapping learning, but to pay more attention to feature extraction and edge weight highlighting. To the best of our knowledge, this is the first time DCT is used to restore degraded depth maps. In short, the use of the DCT module not only simplifies the difficulty of network design, but clarifies the responsibilities of each module, which increases the rationality of model establishment. In addition, we set the tuning parameters in the DCT optimization model learnable during the network update to complete the adaptation to the various input data modalities.

¹The conventional methods here refer to methods that do not use deep learning technology.

Third, to overcome the issue that texture details in RGB images are over-transferred, which leads invalid upsampling guide for depth maps, we employ the enhanced spatial attention (ESA) block from RFANet [18] in our GESA module to highlight the edges in RGB features useful for GDSR. In this way, part of the intensity edges is activated and connected with the depth discontinuities, achieving the selective transfer from the texture structure in guided images.

Fourth, The performances of most GDSR methods [20, 8, 16, 9, 2, 3] are only verified on a limited number of samples, *i.e.*, 5-7 cherry-picked image pairs. However, our method uses a total of 40 image pairs from Middlebury dataset to verify the effectiveness of the model. Qualitative and quantitative experiments implemented can fully prove that our method accurately completes the DGSR task in various scenes and objects. Additional experiments visualized the intermediate products of our model, and a variety of ablation experiments proved the rationality of our model design.

2. Related Work

In this section, we will briefly introduce the GDSR method, and give the difference and connection between the mentioned methods and ours. Note that since SR is a hot topic in computer vision, it contains too many sub-fields and advanced methods. Here we only introduce and analyze the SR methods related to GDSR. In addition, a review of the technologies used in the modules of DCTNet is also given.

2.1. Conventional GDSR methods

In Sec. 1, we have divided the conventional GDSR method into three categories, *i.e.*, filter-, optimization- and learning-based methods.

Filter-based methods. The filter (local) methods aim to use the RGB image to guide the joint filter to perceive the edge in depth map. Starting from Joint bilateral upsampling [14] and its variants [34, 1], RGB image guide the acquisition of bilateral weights. Subsequently, Liu *et al.* [19] replaced the Euclidean distance with the geodesic distances to maintain the discontinuities of the depth image. Weighted mode filter [23], guided filtering [10] and its variants [22, 27] are also widely used in the upsampling process. Lu *et al.* [21] use the smoothing method to process the image parts obtained by the depth map guided RGB image segmentation to solve the texture transferring issue.

Optimization-based methods. The optimization (global) model the interdependency between color image and depth map by Markov Random Field [4], nonlocal means filtering [24], pixel-wise adaptive auto-regressive model [33], total generalized variation [6] and multi-pass optimization framework [17], respectively.

Learning-based methods. Early, bimodal co-sparse analysis [13] and joint dictionaries learning [28] are used to capture the interdependency of RGB/Depth images. A multi-

scale dictionary learning strategy with RGB-D structure similarity measure and a robust coupled dictionary learning algorithm with local coordinate constraints are employed by [15] and [32] to solve over-smoothing and over-fitting problems in information transfer, respectively. Gu *et al.* [8] establish a task-driven learning method to learn the dynamic guidance by a weighted analysis representation model. Xie *et al.* [31] learn an HR edge map inference method from external HR/LR image pair.

2.2. DL-Based GDSR Methods

With the powerful feature extraction capability of DL, GDSR is further developed. Riegler *et al.* [25] adopt the first-order primal-dual algorithm and unroll the optimization processing to a network structure, which establishes the relationship between the DL-based method and the optimized methods category. Li *et al.* [16] establish a two-stream end-to-end network with skip connection to learn the mapping of LR to HR depth maps. Hui *et al.* [12] propose multi-scale guidance for edge transfer. Similarly, Guo [9] use the residual U-Net structure to learn the residual information between bicubic interpolation upsampling and ground truth under multi-scale guidance. The CoAST model [3] based on the iterative shrinkage thresholding algorithm (ISTA) [7] regard the estimation of HR depth map as a linear combination of two LISTA branches. CU-Net [2] set up two modules for separation of common/unique features by multi-modal convolutional sparse coding, and each component design interpretability can be elaborated.

2.3. Compared with related methods

Among the above methods, the most closely related to our method are the optimization category, solving the over-transferred issue category and the DL-based coupled dictionary learning method. (1) The DCT module in our model obtains the depth map features of HR by designing an optimization model, but our method uses DCT to solve the optimization problem for the first time. In addition, the DCT module is integrated into the neural network framework to complete the multi-channel feature acquisition, and the learnable tuning parameters can further enhance the flexibility of the optimization function in the DCT module. (2) For the issue of RGB texture over-transferred, compared to local/global methods, we use advanced ESA module [18] to adaptively learn the edges that need attention in a data-drive scheme. (3) Our feature extraction encoder is inspired by coupled dictionary learning, but we do not need to learn the dictionary explicitly. Instead, the private/shared feature extraction is accomplished by limiting whether the parameters are shared between the convolution kernels.

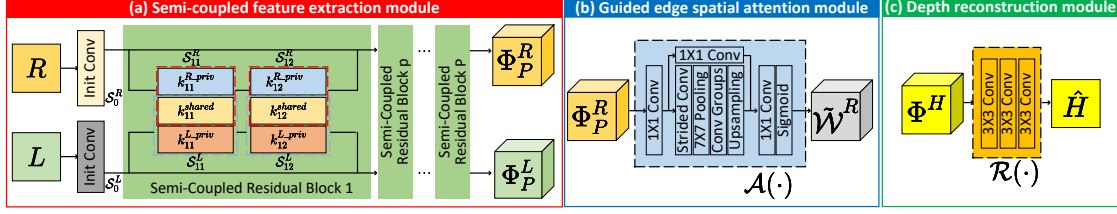


Figure 2. The detailed illustration of DCTNet.

3. Method

In this section, we will elaborate on the specific pipeline and details of our model. For the presentation of DCTNet, we first show how to use DCT to solve an optimization problem we designed, which is used to solve the GDSR task in the image domain. Subsequently, the limitations and challenges of the optimization model are explained. Then we introduce the working pipeline of DCTNet. While introducing the responsibilities of each module, the reasons for how this module can alleviate the challenges presented in the above optimization model and in Sec. 1 are also mentioned. Finally, the details of training loss and model construction are given.

3.1. Model formulation

To start, we first define some important symbols. In the GDSR task, we expect to input the HR RGB image $R \in \mathbb{R}^{M \times N \times 3}$ and the LR depth image $\tilde{L} \in \mathbb{R}^{m \times n}$, where $\{M, N\}$ and $\{m, n\}$ are the height and width of input RGB/depth image, respectively. We aim to obtain the HR depth image $H \in \mathbb{R}^{M \times N}$ under the guidance of R . We then perform the preprocessing operation, where $\tilde{R} \in \mathbb{R}^{M \times N}$ denotes the Y channel in YCrCb color space of R and $L \in \mathbb{R}^{M \times N}$ is the upsampled image of \tilde{L} . As is known to all, GDSR is an ill-posed issue. If R and \tilde{L} in the same scene are given, H can be obtained by minimizing the following optimization function:

$$\mathcal{F} = \frac{1}{2} \|H - L\|_2^2 + \frac{\lambda}{2} \|\mathcal{L}(H) - \mathcal{L}(\tilde{R}) \circ \mathcal{W}(\tilde{R})\|_2^2, \quad (1)$$

where $\mathcal{L}(\cdot)$ is the Laplacian filter, $\mathcal{W}(\cdot)$ can be regarded as a given threshold function to select the edges useful for GDSR. \circ denotes element-wise multiplication and λ is the tuning parameter. The solution can be acquired by $\frac{\partial \mathcal{F}}{\partial H} = 0$, and we have

$$H + \lambda \mathcal{L}^2(H) = \lambda \mathcal{L}^2(\tilde{R}) \circ \mathcal{W}(\tilde{R}) + L. \quad (2)$$

We set $\lambda \mathcal{L}^2(\tilde{R}) \circ \mathcal{W}(\tilde{R}) + L \triangleq E$, then implement DCT operation on both sides of the equation:

$$\mathcal{F}_c(H) + \lambda K^2 \circ \mathcal{F}_c(H) = \mathcal{F}_c(E), \quad (3)$$

where $\mathcal{F}_c(\cdot)$ is the DCT, $K_{ij} = \cos\left(\frac{i-1}{M}\pi\right) + \cos\left(\frac{j-1}{N}\pi\right)$ and $1 \leq i \leq M, 1 \leq j \leq N$. Finally, the HR depth image

are acquired by:

$$H = \mathcal{F}_c^{-1} \{ \mathcal{F}_c(E) \oslash (I + \lambda K^2) \}, \quad (4)$$

where $\mathcal{F}_c^{-1}(\cdot)$ is the inverse DCT operation, \oslash denotes the element-wise division, and I is the identity matrix. More detailed calculation can be referred in the supplementary material.

The above method has the following challenges: (a) Although H can be solved by optimization, it requires additional edge-perceptual methods to determine $\mathcal{W}(\cdot)$. (b) The λ is manually given in Eq. (2), which makes the model only fit for a specific data domain and lacks flexibility. (c) The optimization of a single channel in the image domain is difficult to effectively model the cross-modal internal feature correlation. Combining the possible problems raised in Sec. 1, *i.e.*, RGB texture over-transferred and the difficulty of natural prior learning, we will propose an advanced DCTNet in the next section to alleviate the above problems.

3.2. DCTNet

Our proposed DCTNet consists of four components, *i.e.*, semi-coupled feature extraction (SCFE) module, guided edge spatial attention (GESA) module, discrete cosine transform (DCT) module and depth reconstruction module. The detailed illustration can be seen in Fig. 1 and 2.

First, L and R are paired input into the feature extraction module, and semi-coupled residual blocks are used to extract shared/private features from the source images. The RGB feature is then employed by the GESA module to obtain the attention edge weights useful for SR. Subsequently, multi-channel RGB/depth features and the attention edge weights are input into the DCT module to acquire HR depth features, and the final predicted HR depth map is reconstructed by the depth reconstruction module. The working mechanism of each module will be explained next.

3.2.1 Semi-coupled feature extraction module

We claim that the RGB and depth maps in the same scene will have redundant information (*e.g.*, shape and edges) and complementary information (*e.g.*, RGB texture details and depth image discontinuities). At the same time, based on the basic assumptions of the GDSR that some of the features

contained in the cross-modal image should be interdependent, and some of them should have their own characteristics. Therefore, our SCFE module is set to achieve cross-modal shared/private feature extraction.

We can regard the SCFE module as an encoder for feature extraction, as shown in Fig. 2(a). The internal convolution kernel setting can be regarded as two initial convolution and P semi-coupled residual blocks. Here we denote the initial convolution layer corresponding to $\{L, R\}$ as $\{S_0^L, S_0^R\}$, and the q th convolution layer in the p th semi-coupled residual block corresponding to $\{L, R\}$ is denoted as $\{S_{pq}^L, S_{pq}^R\}$, where $p = 1, 2, \dots, P$ and $q = 1, 2$. The output features of $\{S_{pq}^L, S_{pq}^R\}$ are presented by $\{\Phi_{pq}^L, \Phi_{pq}^R\} \in \mathbb{R}^{M \times N \times C}$, where C is the number of kernels in $\{S_{pq}^L, S_{pq}^R\}$. P and C are determined in Sec 4.1. Note that when $q = 2$, $\{\Phi_{pq}^L, \Phi_{pq}^R\}$ can be abbreviated as $\{\Phi_p^L, \Phi_p^R\}$. The initialization layer completes $\Phi_0^R = S_0^R(R)$, $\Phi_0^L = S_0^L(L)$. Then taking the 1st convolution kernel in the p th semi-coupled residual block as an example, the semi-coupled convolution operation can be expressed as

$$\Phi_{p1}^R(\Phi_{p-1}^R) = \Phi_{p-1}^R * \mathcal{C}(k_{p1}^{shared}, k_{p1}^{R-priv}), \quad (5)$$

$$\Phi_{p1}^L(\Phi_{p-1}^L) = \Phi_{p-1}^L * \mathcal{C}(k_{p1}^{shared}, k_{p1}^{L-priv}), \quad (6)$$

where $*$ represents the convolution operation, $\{k_{p1}^{shared}, k_{p1}^{R-priv}, k_{p1}^{L-priv}\}$ denote the shared convolution kernels with shared parameters and the convolution kernels corresponding to L and R respectively. $\mathcal{C}(\cdot, \cdot)$ denotes the convolution kernel concatenation operation in the channel dimension. Thus, the output feature Φ_p^R of R in the p th residual block is calculated by

$$\Phi_p^R = \text{ReLU} \{S_{p2}^R(\text{ReLU}(S_{p1}^R(\Phi_{p-1}^R))) + \Phi_{p-1}^R\}, \quad (7)$$

and that of Φ_p^L is similar to Eq. (7), only the superscript needs to be replaced from R to L . Finally, the output of SCFE module are Φ_P^L and Φ_P^R , which contain both the shared and the private features in cross-modal input images.

Compared with fully coupled or independent convolution kernel settings, the semi-coupled convolution kernels in the SCFE module can learn the shared/private parts of their respective input features, and extract features more effectively. The verification for the effectiveness of SCFE module can be referred in Sec. 4.3.

3.2.2 Guided edge spatial attention module

To prevent the problem that irrelevant textures are transferred to the HR depth map H when guided RGB image contains rich detail texture information, we use the ESA block from RFANet [18] that achieves excellent results in single image SR task as our GESA module, as shown in Fig. 2(b). We use $\mathcal{A}(\cdot)$ to represent the calculation operation in this module

Determination of network depth P ($C = 64$)					
Metrics	2	3	4	5	6
SSIM	0.9294	0.9424	0.9607	0.9607	0.9607
RMSE	7.333	8.111	5.655	5.695	5.680
PSNR	33.142	31.032	33.785	33.809	33.668
CC	0.9590	0.9670	0.9880	0.9827	0.9830

Determination of network width C ($P = 4$)					
Metrics	8	16	32	64	128
SSIM	0.8980	0.9324	0.9490	0.9607	0.9626
RMSE	10.754	8.031	6.833	5.655	5.661
PSNR	28.524	31.240	32.836	33.785	33.723
CC	0.9370	0.9652	0.9752	0.9880	0.9883

Table 1. Results of the determination for depth P and width C of DCTNet in the validation set. **Bold** indicates the best result.

and the guided edge attention weight can be obtained by $\tilde{\mathcal{W}}^R \in \mathbb{R}^{M \times N} = \mathcal{A}(\Phi_P^R)$.

In this way, part of the edges in intensity features are activated and highlighted. Compared with conventional methods to manually design criteria to extract edge weights useful for upsampling, data-driven methods can achieve adaptive extraction of attention weights.

3.2.3 Discrete cosine transform module

In the above subsections, we have acquired the multi-channel features Φ^R and Φ^L corresponding to L, R^2 , and guided edge attention weight $\tilde{\mathcal{W}}^R$. In this subsection, we will use them to accomplish the depth feature upsampling. In Eq. (4), we illustrate that given a pair of L, R and a threshold functions $\mathcal{W}(\cdot)$, the HR depth image can be reconstructed through DCT operation. Thus we consider DCT algorithm as a module, which can be integrated into DCTNet framework. Furthermore, it can be expanded to obtain the multi-channel HR depth map features by completing the DCT operation on each feature channel. Mathematically, the calculation in DCT module, if we denote it as $\mathcal{DCT}(\cdot, \cdot, \cdot)$, is implemented by

$$\Phi^H = \mathcal{DCT}(\Phi^R, \Phi^L, \tilde{\mathcal{W}}^R), \quad (8)$$

where $\Phi^H \in \mathbb{R}^{M \times N \times C}$ is the guided upsampling feature of depth map L . In detail, $\mathcal{DCT}(\cdot, \cdot, \cdot)$ is expressed as

$$\Phi^E[c] \triangleq \tilde{\lambda}_c \mathcal{L}^2(\Phi^R[c]) \odot \tilde{\mathcal{W}}^R[c] + \Phi^L[c], \quad (9)$$

$$\Phi^H[c] = \mathcal{F}_c^{-1} \left\{ \mathcal{F}_c(\Phi^E[c]) \odot (I + \tilde{\lambda}_c K^2) \right\}, \quad (10)$$

where $\Phi^H[c] \in \mathbb{R}^{M \times N}$ is the c th channel feature map of Φ^H . Notably, compared with the manually given λ in (1) and (4), the $\tilde{\lambda} \in \mathbb{R}^C$ in (10) is set as learnable parameter. It can be

²We abbreviate $\{\Phi_P^L, \Phi_P^R\}$ as $\{\Phi^L, \Phi^R\}$.

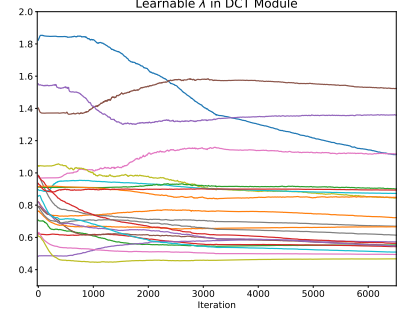
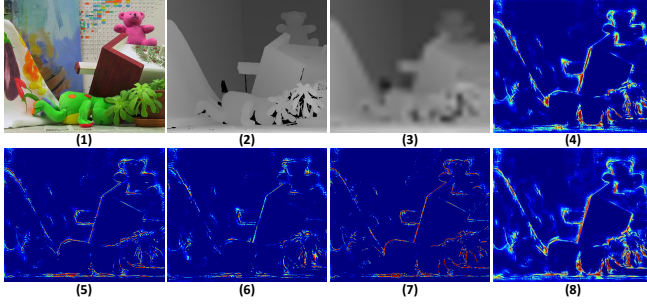


Figure 3. Left: (1)-(3): Input R , ground truth H and Input L , respectively. (4)-(8): Representative highlighting edge weights output by GESA module. Right: Exhibition for the changing curve of learnable parameters $\tilde{\lambda}$ during training. Different colored lines denote $\tilde{\lambda}_c$ corresponding to different channels.

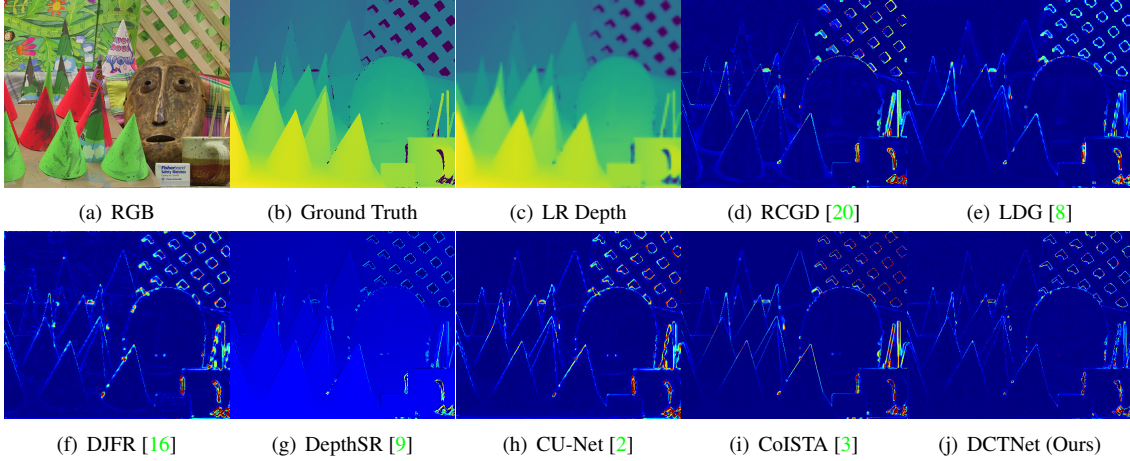


Figure 4. Error maps for visual comparisons of “03-cones4” in $4\times$ upscaling.

updated with iterations, which improves the flexibility of our method.

Therefore, in our DCT module, the acquisition for the feature map Φ^H is learning-free, *i.e.*, it can be uniquely determined by the DCT operation. This design can not only reduce the difficulty of DCTNet design and the size of the network, but also improve the rationality compared to the neural network module established intuitively.

3.2.4 Depth reconstruction module

Finally, the aim of the depth reconstruction module is to predict the HR depth map from its feature map Φ^H , which is the output of the DCT module. The detailed structure is shown in Fig. 2(c). In formula, the function $\mathcal{R}(\cdot)$ of this module can be expressed as $\hat{H} = \mathcal{R}(\Phi^H)$, where $\hat{H} \in \mathbb{R}^{M \times N}$ is the predicted HR depth map of DCTNet.

3.3. Training details

Consistent with [2], we choose ℓ_2 -loss as supervision loss function. That is, $L = \sum_{i=1}^N \|\hat{H}_i - H_i\|_2^2$, where H is the ground truth of depth map.

4. Experiment

Numerous experiments in this section are conducted to prove the effectiveness and rationality of DCTNet.

Datasets, metrics and implement details. We utilize the training set [25] to train our model, and the training samples are resized to 256×256 in the pre-processing stage. The epoch of the network is set to 100, and the batchsize is set to 4. The choice of optimizer is Adam with the default settings. For models with downsampling scales $4\times$, $8\times$ and $16\times$, the learning rate is equal to 10^{-4} , 5×10^{-4} and 10^{-3} , respectively. We choose Middlebury [11] as the validation and test set, which is commonly used in GDSR. The dataset contains a total of 52 paired RGB/Depth images, of which 10 are used as the validation set and 42 are used as the test set. According to the different times of dataset production, we divided the test set into Middlebury-03&05³, Middlebury-06 and Middlebury-14. In the test phase, four metrics including root mean square error (RMSE), structural similarity index (SSIM) [29], signal-to-noise ratio (PSNR) and correlation

³Since Middlebury-03 only contains two pairs of samples, we merge it with Middlebury-05 as Middlebury-03&05 in subsequent experiments.

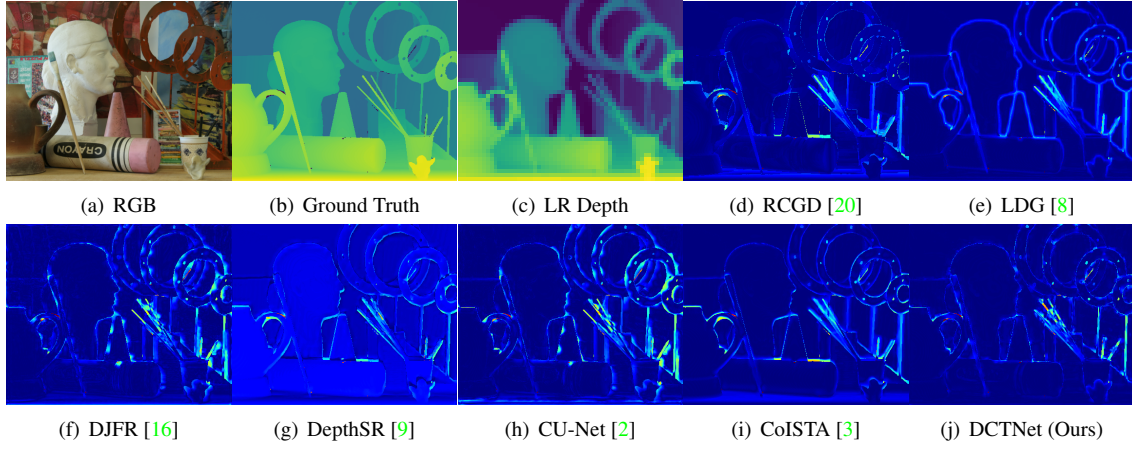


Figure 5. Error maps for visual comparisons of “05-Art” in $8\times$ upscaling.

Scaling factor = 4												
Methods	Middlebury-03&05				Middlebury-06				Middlebury-14			
	SSIM	RMSE	PSNR	CC	SSIM	RMSE	PSNR	CC	SSIM	RMSE	PSNR	CC
RCGD	0.932	8.545	29.612	0.980	0.943	8.438	30.294	0.976	0.942	4.034	36.865	0.971
LDG	<u>0.941</u>	<u>7.647</u>	<u>30.523</u>	<u>0.984</u>	<u>0.957</u>	<u>6.588</u>	<u>32.365</u>	<u>0.985</u>	0.948	<u>3.551</u>	38.006	0.979
DJFR	0.915	9.722	28.496	0.974	0.943	8.189	30.485	0.977	0.945	4.186	36.281	0.968
DepthSR	0.916	10.976	28.393	0.974	0.948	8.289	30.340	0.975	0.948	3.972	36.363	0.969
CU-Net	0.915	9.992	28.285	0.973	0.946	8.202	30.591	0.976	0.946	3.857	37.446	0.975
CoISTA	0.937	8.647	29.569	0.980	0.946	8.880	30.090	0.973	<u>0.955</u>	3.597	<u>38.196</u>	<u>0.979</u>
DCTNet	0.953	7.530	30.660	0.985	0.967	6.433	32.526	0.986	0.963	3.288	38.803	0.982
Scaling factor = 8												
Methods	Middlebury-03&05				Middlebury-06				Middlebury-14			
	SSIM	RMSE	PSNR	CC	SSIM	RMSE	PSNR	CC	SSIM	RMSE	PSNR	CC
RCGD	0.902	11.087	27.369	0.967	0.913	11.667	27.494	0.953	0.926	5.357	34.692	0.954
LDG	0.901	9.833	28.409	0.974	<u>0.922</u>	<u>9.008</u>	<u>29.729</u>	<u>0.972</u>	0.926	<u>4.789</u>	<u>35.629</u>	<u>0.965</u>
DJFR	0.869	12.743	26.165	0.956	0.908	10.585	28.148	0.961	0.905	6.427	32.291	0.930
DepthSR	0.865	12.854	25.066	0.955	0.908	11.364	27.972	0.954	0.905	5.655	32.134	0.945
CU-Net	0.866	13.029	25.991	0.954	0.914	10.399	28.398	0.962	0.909	5.665	33.706	0.947
CoISTA	<u>0.902</u>	11.463	27.137	0.965	0.918	12.195	27.314	0.949	<u>0.930</u>	5.178	35.283	0.961
DCTNet	0.925	<u>10.105</u>	<u>28.217</u>	<u>0.972</u>	0.948	8.801	29.990	0.972	0.939	4.652	35.799	0.965
Scaling factor = 16												
Methods	Middlebury-03&05				Middlebury-06				Middlebury-14			
	SSIM	RMSE	PSNR	CC	SSIM	RMSE	PSNR	CC	SSIM	RMSE	PSNR	CC
RCGD	0.878	13.901	25.458	0.949	0.890	15.149	25.264	0.922	<u>0.914</u>	6.785	32.818	0.932
LDG	0.880	<u>12.215</u>	<u>26.602</u>	<u>0.959</u>	0.897	<u>11.976</u>	<u>27.268</u>	<u>0.951</u>	0.910	6.182	33.538	0.943
DJFR	0.795	19.154	22.626	0.897	0.842	17.850	23.412	0.897	0.808	11.350	27.288	0.829
DepthSR	0.794	19.714	22.765	0.893	0.827	18.956	23.522	0.886	0.801	12.307	26.884	0.907
CU-Net	0.795	19.181	22.643	0.897	0.823	17.604	23.552	0.899	0.638	14.596	25.016	0.825
CoISTA	<u>0.880</u>	14.281	25.240	0.947	<u>0.899</u>	15.616	25.118	0.918	0.912	6.802	<u>33.007</u>	<u>0.935</u>
DCTNet	0.899	12.121	26.639	0.960	0.924	11.626	27.476	0.953	0.915	<u>6.522</u>	32.881	0.934

Table 2. Quantitative results among the SOTA methods and ours in test datasets. The best and the second best values are highlighted by **bold** typeface and underline, respectively.

coefficient (CC) are employed to measure SR image quality. The larger SSIM, PSNR, CC and the smaller RMSE imply the higher quality of predicted depth images. The training and testing are conducted with Pytorch on a computer with Intel Core i9-10900K CPU@3.70GHz and NVIDIA GeForce RTX2080Ti GPU. The initialization of the learnable parameter $\tilde{\lambda}$ equals to e^θ , where $\theta \sim \mathcal{N}(0.1, 0.3)$. The number of semi-coupled residual blocks P and the kernel numbers C of semi-coupled filters in each convolution layer are determined to be 4 and 64, respectively. The specific determination of P and C can refer to the empirical verification experiments in Sec.4.1.

4.1. Empirical validation experiment

Effect of network depth and width. For DCTNet, the depth P and the width C play an important role in the effectiveness of upsampling. We show the results among different combinations of $\{P, C\}$ in the validation set. We first fix $C = 64$, and calculate the image quality when $P = 2, 3, 4, 5, 6$ on the validation set. Then we verify the SR results for $C = 8, 16, 32, 64, 128$ when fixed $P = 4$. The results are demonstrate in Tab. 1. When $P < 4$, the model effect is limited. When $P > 4$, increasing the depth is not obvious to the result. Similarly, when C exceeds 64, there is no significant effect for training costs increasing. To balance model accuracy and computational cost, we believe that $\{P = 4, C = 64\}$ is the best choice.

Effect of highlighting edge weights. We output the first three and last two channels of guided edge attention weights $\tilde{\mathcal{W}}^R$ from a representative sample in Fig. 3. Obviously, after the attention weight purification of the GESA module, the edge contour of the object is effectively highlighted and the texture information inside the object is eliminated, which can alleviate the issue for texture over-transferred and benefit the GDSR operation.

Effect of learnable parameters. One of our claims is that when our tuning parameter $\tilde{\lambda}$ in (10) becomes a sequence of learnable parameters, the flexibility of our model is further improved. Here we show the changing curve of $\tilde{\lambda}$ on each channel corresponding to the iteration number during the training phase in Fig. 3. It can be found that under the data-driven scheme, $\tilde{\lambda}$ will be adaptive to different importance of the fidelity term and the regular term. Compared with the manually given λ in (4), our method is more suitable for the characteristics of different data domains.

4.2. Comparison with SOTA methods

To further prove the effectiveness of our method, we compare results of DCTNet on the test set with state-of-the-art methods, including RCGD [20], LDG [8], DJFR [16], DepthSR [9], CU-Net [2] and CoSTA [3]. The qualitative results of the comparisons are shown in Fig.4-5. Intuitively, our depth prediction results have lower prediction errors,

	SSIM	RMSE	PSNR	CC
Exp. 1	0.945	6.663	32.526	0.987
Exp. 2	0.919	7.086	31.123	0.960
Exp. 3	0.915	6.998	31.232	0.979
Exp. 4	0.935	6.916	31.271	0.965
Exp. 5	0.935	7.916	31.371	0.965
Ours	0.961	5.618	34.233	0.983

Table 3. Results of ablation experiments in the total testset of Middlebury. **Bold** indicates the best result.

which are closer to the ground truth images. More visual comparisons are placed in the supplementary material. The quantitative results are exhibited in Tab. 2. Our method has excellent performance under multiple datasets and different downsampling scales, showing that our method is suitable for different objects and imaging conditions, and can surpass SOTA methods.

4.3. Ablation experiments

We verify the rationality of modules in DCTNet through ablation experiments, and the results are demonstrated in Tab. 3. Note that the specific network structure in Exp. 3 and 5 can be found in supplementary material.

Semi-coupled filters. We change the coupling degree of convolution kernels into independent (Exp. 1) and fully coupled (Exp. 2) cases, respectively. For Exp. 1, The result proves that the ability of unrestricted kernels to extract features is weaker than that of semi-coupled filters, and it is more difficult to train an effective shared feature extractor without coupled kernels. For Exp. 2, considering that images from different modalities have distinct features, fully coupled filters lead to poor results if the cross-modality disparity is not taken into account.

The DCT module. In Exp. 3, we remove the DCT module and employ a three-layer convolutional framework to learning the mapping in (8). Obviously, the removal of the DCT module not only increases the number of learnable parameters, but reduces the prediction accuracy, which proves the rationality of DCT module based on the optimization model.

Learnable parameters $\tilde{\lambda}$. We fixed $\tilde{\lambda}$ to $e^{0.1}$ in Exp. 4, which is the mean value of its initialization. It is proved that a fixed tuning coefficient will reduce the flexibility of the model and reduce the ability of SR.

Residual skip connection. In Exp. 5, we removed the residual connection in SCFE module and only used the simple stacking of convolution kernels. We get that the residual connection has a more obvious effect on feature extraction, which is helpful for network training.

5. Conclusion

This paper establishes a guided depth map super-resolution model based on discrete cosine transform, semi-coupled convolution feature extraction and edge attention mechanism. We reasonably extended the solution of optimization model based on discrete cosine transform to a deep learning module, and combined with effective shared/private feature extraction and data-driven guided edge attention mechanism learning, alleviating the issues for RGB texture over-transferred, cross-modal feature extraction difficulty and unclear working mechanism of modules in existing methods. The effectiveness of our model is fully proved by various qualitative and quantitative comparisons.

References

- [1] Massimo Camplani, Tomás Mantecón, and Luis Salgado. Depth-color fusion strategy for 3-d scene modeling with kinect. *IEEE Trans. Cybern.*, 43(6):1560–1571, 2013. 2, 3
- [2] X. Deng and P. L. Dragotti. Deep convolutional neural network for multi-modal image restoration and fusion. *IEEE Transactions on Pattern Analysis and Machine Intelligence*, pages 1–1, 2020. 2, 3, 6, 7, 8
- [3] Xin Deng and Pier Luigi Dragotti. Deep coupled ISTA network for multi-modal image super-resolution. *IEEE Trans. Image Process.*, 29:1683–1698, 2020. 2, 3, 6, 7, 8
- [4] James Diebel and Sebastian Thrun. An application of markov random fields to range sensing. In *NIPS*, pages 291–298, 2005. 2, 3
- [5] Chao Dong, Chen Change Loy, Kaiming He, and Xiaoou Tang. Learning a deep convolutional network for image super-resolution. In *ECCV (4)*, volume 8692 of *Lecture Notes in Computer Science*, pages 184–199. Springer, 2014. 1
- [6] David Ferstl, Christian Reinbacher, René Ranftl, Matthias Rütger, and Horst Bischof. Image guided depth upsampling using anisotropic total generalized variation. In *ICCV*, pages 993–1000. IEEE Computer Society, 2013. 2, 3
- [7] Karol Gregor and Yann LeCun. Learning fast approximations of sparse coding. In *ICML*, pages 399–406. Omnipress, 2010. 3
- [8] Shuhang Gu, Wangmeng Zuo, Shi Guo, Yunjin Chen, Chongyu Chen, and Lei Zhang. Learning dynamic guidance for depth image enhancement. In *CVPR*, pages 712–721. IEEE Computer Society, 2017. 2, 3, 6, 7, 8
- [9] Chunle Guo, Chongyi Li, Jichang Guo, Runmin Cong, Huazhu Fu, and Ping Han. Hierarchical features driven residual learning for depth map super-resolution. *IEEE Trans. Image Process.*, 28(5):2545–2557, 2019. 2, 3, 6, 7, 8
- [10] Kaiming He, Jian Sun, and Xiaoou Tang. Guided image filtering. *IEEE Trans. Pattern Anal. Mach. Intell.*, 35(6):1397–1409, 2013. 3
- [11] Heiko Hirschmüller and Daniel Scharstein. Evaluation of cost functions for stereo matching. In *CVPR*. IEEE Computer Society, 2007. 6
- [12] Tak-Wai Hui, Chen Change Loy, and Xiaoou Tang. Depth map super-resolution by deep multi-scale guidance. In *ECCV (3)*, volume 9907 of *Lecture Notes in Computer Science*, pages 353–369. Springer, 2016. 2, 3
- [13] Martin Kiechle, Simon Hawe, and Martin Kleinsteuber. A joint intensity and depth co-sparse analysis model for depth map super-resolution. In *ICCV*, pages 1545–1552. IEEE Computer Society, 2013. 2, 3
- [14] Johannes Kopf, Michael F. Cohen, Dani Lischinski, and Matthew Uyttendaele. Joint bilateral upsampling. *ACM Trans. Graph.*, 26(3):96, 2007. 2, 3
- [15] HyeokHyen Kwon, Yu-Wing Tai, and Stephen Lin. Data-driven depth map refinement via multi-scale sparse representation. In *CVPR*, pages 159–167. IEEE Computer Society, 2015. 2, 3
- [16] Yijun Li, Jia-Bin Huang, Narendra Ahuja, and Ming-Hsuan Yang. Joint image filtering with deep convolutional networks.

- IEEE Trans. Pattern Anal. Mach. Intell.*, 41(8):1909–1923, 2019. 2, 3, 6, 7, 8
- [17] Yu Li, Dongbo Min, Minh N. Do, and Jiangbo Lu. Fast guided global interpolation for depth and motion. In *ECCV (3)*, volume 9907 of *Lecture Notes in Computer Science*, pages 717–733. Springer, 2016. 2, 3
- [18] Jie Liu, Wenjie Zhang, Yuting Tang, Jie Tang, and Gangshan Wu. Residual feature aggregation network for image super-resolution. In *CVPR*, pages 2356–2365. IEEE, 2020. 1, 3, 5
- [19] Ming-Yu Liu, Oncel Tuzel, and Yuichi Taguchi. Joint geodesic upsampling of depth images. In *CVPR*, pages 169–176. IEEE Computer Society, 2013. 2, 3
- [20] Wei Liu, Xiaogang Chen, Jie Yang, and Qiang Wu. Robust color guided depth map restoration. *IEEE Trans. Image Process.*, 26(1):315–327, 2017. 3, 6, 7, 8
- [21] Jiajun Lu and David A. Forsyth. Sparse depth super resolution. In *CVPR*, pages 2245–2253. IEEE Computer Society, 2015. 2, 3
- [22] Jiangbo Lu, Keyang Shi, Dongbo Min, Liang Lin, and Minh N. Do. Cross-based local multipoint filtering. In *CVPR*, pages 430–437. IEEE Computer Society, 2012. 2, 3
- [23] Dongbo Min, Jiangbo Lu, and Minh N. Do. Depth video enhancement based on weighted mode filtering. *IEEE Trans. Image Process.*, 21(3):1176–1190, 2012. 2, 3
- [24] Jaesik Park, Hyeonwoo Kim, Yu-Wing Tai, Michael S. Brown, and In-So Kweon. High quality depth map upsampling for 3d-tof cameras. In *ICCV*, pages 1623–1630. IEEE Computer Society, 2011. 2, 3
- [25] Gernot Riegler, David Ferstl, Matthias Rüther, and Horst Bischof. A deep primal-dual network for guided depth super-resolution. In *BMVC*. BMVA Press, 2016. 2, 3, 6
- [26] Gernot Riegler, Matthias Rüther, and Horst Bischof. Atgv-net: Accurate depth super-resolution. In *ECCV (3)*, volume 9907 of *Lecture Notes in Computer Science*, pages 268–284. Springer, 2016. 1
- [27] Xiao Tan, Changming Sun, and Tuan D. Pham. Multipoint filtering with local polynomial approximation and range guidance. In *CVPR*, pages 2941–2948. IEEE Computer Society, 2014. 3
- [28] Ivana Tomic and Sarah Drewes. Learning joint intensity-depth sparse representations. *IEEE Trans. Image Process.*, 23(5):2122–2132, 2014. 2, 3
- [29] Zhou Wang, Alan C. Bovik, Hamid R. Sheikh, and Eero P. Simoncelli. Image quality assessment: from error visibility to structural similarity. *IEEE Trans. Image Process.*, 13(4):600–612, 2004. 6
- [30] Huikai Wu, Shuai Zheng, Junge Zhang, and Kaiqi Huang. Fast end-to-end trainable guided filter. In *CVPR*, pages 1838–1847. IEEE Computer Society, 2018. 2
- [31] Jun Xie, Rogério Schmidt Feris, and Ming-Ting Sun. Edge-guided single depth image super resolution. *IEEE Trans. Image Process.*, 25(1):428–438, 2016. 1, 2, 3
- [32] Jun Xie, Rogério Schmidt Feris, Shiaw-Shian Yu, and Ming-Ting Sun. Joint super resolution and denoising from a single depth image. *IEEE Trans. Multim.*, 17(9):1525–1537, 2015. 2, 3
- [33] Jingyu Yang, Xinchun Ye, Kun Li, Chunping Hou, and Yao Wang. Color-guided depth recovery from RGB-D data using an adaptive autoregressive model. *IEEE Trans. Image Process.*, 23(8):3443–3458, 2014. 2, 3
- [34] Qingxiong Yang, Ruigang Yang, James Davis, and David Nistér. Spatial-depth super resolution for range images. In *CVPR*. IEEE Computer Society, 2007. 3
- [35] Kai Zhang, Wangmeng Zuo, Shuhang Gu, and Lei Zhang. Learning deep CNN denoiser prior for image restoration. In *CVPR*, pages 2808–2817. IEEE Computer Society, 2017. 2